Diabetes-Impaired Wound Healing Is Improved by Matrix Therapy with Heparan Sulfate Glycosaminoglycan Mimetic OTR4120 in Rats

Miao Tong[1], Bastiaan Tuk[1], Peng Shang[2], Ineke M. Hekking[1], Esther M.G. Fijneman[1], Marnix Guijt[1], Steven E.R. Hovius[1], Johan W. van Neck[1]

[1]Department of Plastic and Reconstructive Surgery, Erasmus MC, University Medical Center, Rotterdam, the Netherlands

[2]Department of Reproduction and Development, Erasmus MC, University Medical Center, Rotterdam, the Netherlands

Corresponding Author:

M. Tong

Dept. of Plastic and Reconstructive Surgery,

Erasmus MC, University Medical Center, Room Ee 15.89,

P.O. Box 2040, 3000 CA Rotterdam, the Netherlands,

Tel: +31-10-7043242, Fax: +31-10-7044685;

Email: m.tong@hotmail.com

Running Title: HS-GAG mimetic improves diabetic ulcer healing

WORD COUNT: 2971

NUMBER OF FIGURES: 8

ABSTRACT

Wound healing in diabetes is frequently impaired and its treatment remains a challenge. We tested a therapeutic strategy of potentiating intrinsic tissue regeneration by restoring the wound cellular environment using a heparan sulfate glycosaminoglycan mimetic, OTR4120. The effect of OTR4120 on healing of diabetic ulcers was investigated. Experimental diabetes was induced by intraperitoneal injection of streptozotocin. Seven weeks after induction of diabetes, rats were ulcerated by clamping a pair of magnet disks on the dorsal skin for 16 h. After magnet removal, OTR4120 was administered via an intramuscular injection weekly for up to 4 weeks. To examine the wound healing in OTR4120-treated rats, the degree of ulceration, inflammation, angiogenesis, and collagen synthesis were evaluated. We found that OTR4120 significantly reduced the degree of ulceration and the time of healing. These effects were associated with reduced neutrophil infiltration and macrophage accumulation, and enhanced angiogenesis. OTR4120 treatment also increased the collagen content with an increase of collagen type I biosynthesis and reduction of collagen type III biosynthesis. Moreover, restoration of the ulcer biomechanical strength was significantly enhanced following OTR4120 treatment. This study shows that matrix therapy with OTR4120 improves diabetes-impaired wound healing.

Impaired wound healing is a well-documented phenomenon both in experimental and clinical diabetes [1]. Several mechanisms for diabetes-impaired wound healing are proposed that are mostly related to impairment of macrophage function [2], angiogenic response [3], and extracellular matrix (ECM) deposition [4]. The ideal treatment relies on

correcting the multiple deficits simultaneously through highly integrated and personalized therapeutic approaches.

Wound healing is associated with dynamic interactions between ECM and growth factors (GFs) [5]. The ECM consists of a network of scaffold proteins that are bridged by glycosaminoglycans (GAGs), of which heparan sulfate (HS) is an important component. HS-GAGs are capable of transmitting signals by providing binding sites for a large variety of HS-bound signaling peptides(i.e., GFs, chemokines, and cytokines). However, following tissue injury, the glycanases and proteases can destroy HS-GAGs [6]. As a result, the ECM-GFs interactions are disturbed. These disruptions characterize impaired wounds [5, 7] and also may have the implication of matrix therapy.

OTR4120 is a HS-GAG mimetic that can replace the degraded HS-GAGs, and protect and improve the bioavailability of GFs, cytokines and other heparin binding signaling peptides. In this way, OTR4120 offers a matrix therapy that restores the natural cellular microenvironment and the endogenous signaling of cell communications needed for tissue regeneration (Rouet, 2006)(Rouet, 2005) (Barritault, 2006). This facilitates the quality of healing by potentiating the intrinsic tissue regeneration.

The present study evaluates the efficacy of matrix therapy with OTR4120 in pressure ulcers generated in streptozotocin (STZ)-induced diabetic rats.

RESEARCH DESIGN AND METHODS

Animals. 142 ten-week-old WAG/RijHsd female rats were purchased from Harlan (Zeist, the Netherlands). Rats were exposed to a 12 h light/dark cycle and fed a standard laboratory diet with food and water available *ad libitum*. All procedures with animals were approved by the local Animal Experiments Committee.

Induction of diabetes mellitus. After overnight fasting, animals were given an intraperitoneal injection of STZ (Sigma, St. Louis, MO, USA) at a dose of 65 mg/kg body weight in 0.1 M acetate buffer, pH 4.5. Blood glucose concentration was monitored weekly by a One Touch™ Glucometer (LifeScan, Milpitas CA, USA) from tail vein blood. A prolonged diabetic status was defined as blood glucose levels ≥ 20 mmol/L throughout the induction period.

Ulceration model and OTR4120 treatment. Seven weeks after STZ injection, 119 diabetic rats were obtained and ulcerated by clamping and then removal of a pair of magnet disks (15 mm diameter) on rat dorsal skin for a single ischemic period of 16 h. Following wounding, rats were randomly allocated to 6 groups to serve 6 experimental end points (i.e. day 3, n=16; day 7, n=18; day 14, n=18; day 18, n=15; day 42, n=34, and day 84, n=18). Lyophilized OTR4120 was rehydrated in a physiological salt solution (Braun Melsungen AG, Germany) at a concentration of 1mg/ml. Immediately after magnet removal, rats were randomly assigned to receive an intramuscular injection of OTR4120 in the thigh at a dose of 1 mg/ kg bodyweight or a same volume of physiological salt solution weekly up to one month. The OTR4120 dosage was based on the experience from the previous studies (Garcia-Filipe et al., 2007; Tong et al., 2008; Tong et al., 2009; Tong et al., 2011; Zuijdendorp et al., 2008). At each experimental end

point, the animals were sacrificed simultaneously. The experiment was blinded to all observers.

Macroscopic analysis. Body weight and blood glucose levels were measured and the ulcers were photographed. The ulcers were graded according to the grading system of the National Pressure Ulcer Advisory Panel (NPUAP) [8]. The percentage of completely closed ulcers was calculated.

Immunohistochemistry. Paraffin-embedded sections (5um) were deparaffinized and rehydrated. Antigen retrieval was performed in TE buffer containing 0.1% trypsin (Invitrogen, Carlsbad, CA, USA). Endogenous peroxidase activity was quenched by exposing to 0.1% hydrogen peroxide in phosphate-buffered saline (PBS) containing 0.1% Tween 20 (PBST). After blocking with 4% non-fat milk powder in PBST, the sections were incubated with mouse anti-CD68 (1:100; AbD Serotec, Düsseldorf, Germany) and goat anti-CD34 (1:200; R&D Systems, Minneapolis, MN, USA), respectively, and followed by incubating with the corresponding biotinylated secondary antibodies (R&D systems, Minneapolis, MN, USA). The antigen-antibody complex was detected by streptavidin-peroxidase (R&D systems) and 3,3′-diaminobenzidine (Dako, Carpinteria, CA, USA). For evaluation of staining, the overview of the positive-signal density was scored semi-quantitatively as 1 (absent), 2 (low), 3 (medium), 4 (strong), and 5 (very strong). The medium of scores from three observers, who were blinded to the treatment, was used for comparisons.

Myeloperoxidase assay. Myeloperoxidase (MPO) activity in ulcer tissue homogenates was assayed as previously described with minor modifications [9]. Briefly, homogenates were mixed in 100 mM sodium acetate buffer containing 0.5% hexadecyl trimethyl

ammonium bromide (HETAB) (Sigma, MO, USA). The mixture was centrifuged to extract the MPO. Following centrifugation, the supernatant was incubated at 37 ºC for 15 min in 100 mM sodium acetate buffer, containing 0.0005% hydrogen peroxide, 3.2 mM 3,3′,5,5′-tetramethylbenzidine dihydrochloride (Sigma), and 0.5% HETAB. The optical densities were recorded at 660 nm. MPO content was determined as units per gram tissue homogenate by using a standard curve generated by purified MPO from human leukocytes (Sigma).

Western blot analysis. Protein contents of vascular endothelial growth factor (VEGF), platelet-derived growth factor (PDGF), transforming growth factor beta-1 (TGF-β_1), and inducible nitric oxide synthase (iNOS) in ulcer tissue homogenates were evaluated by Western blot as described previously [10]. Briefly, the protein concentrations of homogenates were determined using RcDc protein assay kit (Bio-Rad, Hercules, CA, USA). Equivalent amount of proteins was separated on a SDS polyacrylamide gel, and transferred onto a polyvinylidene difluoride membrane (Bio-Rad). Blocking was performed in 3 % bovine serum albumin (Sigma) in 10 mM Tris, 150 mM NaCl, containing 0.1% Tween-20. The membranes were probed with 1:1000 diluted mouse anti -VEGF (Santa Cruz Biotechnology, Santa Cruz, CA, USA), 1: 400 diluted rabbit anti-PDGF (Santa Cruz Biotechnology), 1:500 diluted mouse anti-TGF-β1 (R&D Systems, Minneapolis, MN, USA), and 1:400 diluted rabbit anti-iNOS (Calbiochem, San Diego, CA, USA), respectively. Binding of the primary antibody was detected using a peroxidase-conjugated secondary antibody (Pierce, Rockford, IL, USA). Positive bands were visualized using chemiluminescence (Supersignal®, Pierce)

Hydroxyproline content and collagen type I, type III ex vivo biosynthesis measurements. Ulcer biopsies were labeled with 50 mCi (^{3}H) hydroxyproline (GE Healthcare, Diegem, Belgium) for 24 h in Dulbecco's modified Eagle's minimal essential medium supplemented with 100 IU/mL penicillin, 100 mg/mL streptomycin and 2 mM glutamine. The tissue was then washed extensively until no radioactivity was detected. Subsequently, the labeled biopsies were homogenized and a small aliquot of the homogenates was hydrolyzed in 6 N HCl at 100°C for 24 h. The total collagen content was determined by colorimetric hydroxyproline assay [11]. All remaining homogenates were digested with 1% pepsin (Sigma) in 0.5M acetic acid for 48 h. Following centrifugation, the supernatant was dialyzed against 0.5M acetic acid for 24 h and then lyophilized. Before lyophilization, the total pepsin-soluble biosynthesized collagen was measured by determining the amount of (^{3}H) hydroxyproline in the dialysates. Biosynthesis of collagen type I and III was determined following electrophoresis of a 1 mg lyophilized sample on SDS-PAGE. The collagen bands were revealed by Coomassie Brilliant Blue staining and identified by comparison with standard collagen type I and type III. The relative proportions of radioactivity incorporated in collagen types were quantified by excision of each individual collagen band followed by hydrolysis of the band in 6N HCl at 100ºC for 24 h after which (^{3}H) hydroxyproline was determined in the hydrolysate [12].

Breaking strength measurement. Breaking strength was measured as described previously [13]. Briefly, the excised dorsal pelt, containing an ulcer was cut into two standardized dumbbell-shaped skin strips. One strip was centered by a segment of ulcer, and the other was cut from the surrounding normal skin. The strip was fixed

perpendicularly between the two clips of a tensiometer and subjected to a constant strain rate of 60mm/min using a 1.0kg force transducer. Breaking strength was recorded as the maximum load (Newton) measured before skin failure. The ratio of ulcer breaking strength to that of surrounding normal skin breaking strength was calculated for data analysis.

Real-Time Quantitative-PCR

Total RNA from tissues was isolated using TRIzol reagent (Invitrogen, CA, USA). Five micrograms of total RNA was treated for 15 min with DNase I prior to a 50 min reverse transcription reaction using a SuperScript II RT kit (Invitrogen). Quantitative PCR was performed with a SYBR Green PCR Master Mix (Applied Biosystems, CA, USA) using a C1000 Thermal Cycler (BIO-RAD). Melting curves were used as quality controls to exclude samples with genomic DNA content and to ensure single product amplification. Beta-actin levels were used for internal normalization. Data were analyzed with the CFX Manager 2.1 software package (BIO-RAD). The primer sets are described as follows: VEGF-A, Forward 5'-ACGTCACTATGCAGATCATGC-3', Reverse 5'-CCTTTCCCTTTCCTCGAACTG-3'; TGF-β1, Forward 5' CAATTCCTGGCGTTACCTTG3', Reverse 5' AAAGCCCTGTATTCCGTCTC3'; iNOS, Forward 5'-GAACTCGGGCATACCTTCAG-3', Reverse 5'-CTCCCAGGTGAGACAGTTTC-3'.

Statistical analysis. Data are presented as means ± standard error of the mean (SEM). Statistical calculations were performed using SPSS software (version 11, Chicago, IL, USA). The Mann-Whitney U-test was carried out to compare results between groups. A p-value ≤ 0.05 was considered to indicate a statistically significant difference.

RESULTS

Diabetes induction. During the 7-week diabetes induction period, 84% of the STZ-injected rats became consistently hyperglycemic and were included in this study. Of the STZ-injected rats, 7% had glucose levels ≤ 20 mmol/L, 5% died, and 4% were euthanized due to a bodyweight loss of ≥ 10 g/week.

Bodyweight changes. During the diabetes induction period the rats had a weight reduction of up to 17% (Fig. 1). Following STZ injection, from 78 days onwards the average weight restoration was (almost significantly) higher in the OTR4120-treated rats than in control rats (87% vs. 80% on day 78, p=0.08; 90% vs. 81% on day 85, p=0.02; 91% vs. 83% on day 99, p=0.08; and 87% vs. 77% on day 134, *p*=0.06) (Fig. 1).

OTR4120 treatment reduced the degree of ulceration. OTR4120-treated ulcers had significantly lower NPUAP grades compared with control ulcers on day 14 (1.68 ± 0.23 vs. 2.50 ± 0.25, $p < 0.05$).

OTR4120 treatment accelerated ulcer healing. Figure 2 shows that 90% of OTR4120-treated ulcers were completely closed on day 23 after compression release, compared with 50% of control ulcers ($p < 0.05$). All OTR4120-treated ulcers were completely closed on day 42 whereas, 14% of control ulcers were still open ($p < 0.05$). All control ulcers were completely closed on day 49.

OTR4120 treatment reduced neutrophil infiltration and stimulated inflammation resolution. MPO activity was 28% lower in the OTR4120-treated rats compared with control rats on day 3 ($p < 0.01$), and 48% lower on day 7 ($p < 0.05$) (Fig. 3). CD68-staining was detectable during the entire observation period. However, significantly

reduced CD68 staining was found in OTR4120-treated ulcers on days 7, 14 and 84 (Fig. 4).

OTR4120 treatment-enhanced angiogenesis. The density score of CD34 staining in OTR4120-treated ulcers was significantly higher than in controls on day 14 (3.85 ± 0.22 vs. 2.94 ± 0.21, $p < 0.01$) and on day 42 (2.99 ± 0.14 vs. 2.41 ± 0.16, $p < 0.01$) (Fig. 5). The presence of VEGF was 197% higher in OTR4120-treated ulcers than in controls on day 14 ($p < 0.05$) (Fig. 6 A, D). TGF-β_1 was 72% higher in OTR4120-treated ulcers than in controls on day 3 ($p < 0.01$) and 40% higher on day 14 ($p < 0.01$) (Fig. 6 B, E). All scores had reduced to control levels on day 84.

OTR4120 treatment revealed more iNOS. In OTR4120-treated ulcers the presence of iNOS was 66% higher on day 3 (4.04 ± 0.46 vs. 2.43 ± 0.52, $p < 0.05$) and 88% higher on day 14 (5.40 ± 0.87 vs. 2.87 ± 0.35, $p < 0.05$) compared with controls (Fig. 6 C, F).

OTR4120 treatment enhanced breaking strength. The skin strength ratio in OTR4120-treated ulcers was 160% higher on day 18, 33% higher on day 42, and 33% higher on day 84 compared with controls (Fig. 7).

OTR4120 treatment increased hydroxyproline content. The hydroxyproline (OHP) content was increased in OTR4120-treated ulcers compared with controls on day 7 (9.81 ± 0.34 µg OHP/mg homogenate vs. 6.89 ± 0.42 µg OHP/mg homogenate, $p < 0.05$), and on day 42 (14.31 ± 1.11 µg OHP/mg homogenate vs. 10.18 ± 1.01 µg OHP/mg homogenate, $p < 0.05$).

OTR4120 treatment increased ex vivo biosynthesis of collagen type I and reduced collagen type III. The percentage of synthesized type I collagen was significantly increased in OTR4120-treated ulcers on day 42 (92.1 ± 1.36 vs. 86.9 ± 1.57, $p < 0.05$)

(Fig. 8A). In contrast, type III collagen synthesis was reduced in OTR4120-treated ulcers on day 7 and day 42 (9.1 ± 1.00 vs. 12.4 ± 1.10 on day 7, p=0.07; 4.86 ± 1.26 vs. 9.75 ± 1.47 on day 42, $p < 0.05$) (Fig.8 B). The ratio of collagen type I to type III in the OTR4120-treated ulcers was increased twofold compared with control ulcers on day 42 (32.8 ± 7.43 vs. 11.57 ± 3.07, $p < 0.05$) (Fig. 8 C).

OTR4120 treatment had no effect on VEGF-A, TGF-β_1, and iNOS gene transcription. No statistical differences in VEGF-A, TGF-β1, and iNOS gene transcription were found between OTR4120-treated and control groups.

DISCUSSION

Matrix therapy aims to facilitate and potentiate the intrinsic tissue self-regeneration capability by restoring the natural wound micro-environment. In this study, we demonstrate matrix therapy with OTR4120 reduces diabetic ulcer healing time, improves healing quality by reducing inflammation, increasing angiogenesis, reducing collagen type III, enhancing the ulcer biomechanical strength restoration, and weight restoration.

Excess inflammation, associated with a prolonged persistence of neutrophil infiltration, is a consistent feature of diabetes-impaired wound healing [6]. In another study using the same wound model in normal rats, macrophages were only detectable during the first 6 weeks after wounding [14], whereas in the present study macrophages were detectable during the entire 12-week observation period. This is an additional sign that inflammation resolution in diabetic wound healing is impaired. This impaired resolution is stimulated following OTR4120 treatment. Possible mechanisms of the anti-inflammatory properties of OTR4120 might include its effect on inhibiting plasmin and neutrophil elastase

activity [15-16], and increasing the content of TGF-β1 and VEGF that is demonstrated in this study. VEGF is known to induce macrophage apoptosis through stimulation of a tumor necrosis factor [17]. The observed increase of TGF-β1 and VEGF in wounds of OTR4120-treated animals without an OTR4120 effect on TGF-β1 and VEGF gene transcription further strengthens their sequestering/protecting/stabilizing role on GFs. Increased amounts of collagen type III relative to collagen type I are often associated with excessive scarring during tissue remodeling [18]. Ex vivo radio-labeling of collagen allowed us to compare the relative rates of biosynthesis of different collagen types that are thought to reflect collagen synthesis in the wounds directly before sampling. We observed that OTR4120 treatment reduced collagen type III synthesis and increased collagen type I synthesis in the late stages of wound healing. The anti-fibrotic effects of OTR4120 have been reported in healing Crohn's disease intestinal biopsies [19] and burned rat skin [12]. This effect is consistent with the increased ulcer breaking strength after OTR4120 treatment. However, the underlying mechanisms of OTR4120 in regulating the relative proportion of collagen type I and type III during matrix remolding remains unclear.

In addition to the anti-inflammatory and anti-fibrotic effects of OTR4120, this treatment also induced NO production. The diffusible, gaseous molecule NO participates in the orchestration of wound healing by modulating cytokines which are involved in wound healing [20]. NO deficiency is an important mechanism for diabetes-impaired wound healing [20-21]. Most cell types associated with wound healing are capable of producing NO through the activity of nitric oxide synthases (NOSs). iNOS is calcium independent

and controlled by inflammatory cytokines. Once iNOS has induced the production of NO, the content of NO within tissues can increase over 1,000 fold [21].

The above data showed that OTR4120 treatment revealed a positive effect on wound healing. The enhanced wound healing is often an indicator of satisfactory nutritional status and weight gain. The weight restoration was found near significantly improved after OTR4120 treatment. This improved weight gain may contribute to the regenerating effects of OTR4120 treatment on ulcer healing.

In summary, this study shows that a synthetic HS-GAG mimetic OTR4120 accelerates and improves diabetic pressure ulcer healing in rats. Therefore, OTR4120 treatment is a promising matrix therapy for diabetes-impaired wounds.

ACKNOWLEDGMENTS

M.T. researched data and wrote the manuscript. B.T. researched data and edited the IHC images. P.S., I.M.H., E.M.G.F., and M.G. researched data. S.E.R.H. contributed to the discussion. J.W.V.N. researched data and edited the manuscript. All co-authors also have reviewed the manuscript.

The authors thank Dr. V. Barbier and Dr. P. Kern from Laboratoire de Recherches sur la Croissance Cellulaire of Université Paris 12 for their help in collagen biosynthesis measurements and OTR3 (Paris, France) for providing OTR4120.

Dr. Johan W. van Neck is the guarantor of this work and, as such, had full access to all of the data in the study and takes responsibility for the integrity of the data and the accuracy

of the data analysis.

This research was supported by a grant from the Nuts Ohra Foundation (the Netherlands).

REFERENCES

1. Lioupis, C., *Effects of diabetes mellitus on wound healing: an update.* J Wound Care, 2005. **14**(2): p. 84-6.
2. Maruyama, K., et al., *Decreased macrophage number and activation lead to reduced lymphatic vessel formation and contribute to impaired diabetic wound healing.* Am J Pathol, 2007. **170**(4): p. 1178-91.
3. Galiano, R.D., et al., *Topical Vascular Endothelial Growth Factor Accelerates Diabetic Wound Healing through Increased Angiogenesis and by Mobilizing and Recruiting Bone Marrow-Derived Cells.* Am J Pathol, 2004. **164**(6): p. 1935-1947.
4. Lobmann, R., et al., *Expression of matrix-metalloproteinases and their inhibitors in the wounds of diabetic and non-diabetic patients.* Diabetologia, 2002. **45**(7): p. 1011-6.
5. Schultz, G.S. and A. Wysocki, *Interactions between extracellular matrix and growth factors in wound healing.* Wound Repair Regen, 2009. **17**(2): p. 153-62.
6. Eming, S.A., T. Krieg, and J.M. Davidson, *Inflammation in wound repair: molecular and cellular mechanisms.* J Invest Dermatol, 2007. **127**(3): p. 514-25.
7. Menke, N.B., et al., *Impaired wound healing.* Clin Dermatol, 2007. **25**(1): p. 19-25.
8. Lardenoye, J.W., J.A. Thiefaine, and P.J. Breslau, *Assessment of incidence, cause, and consequences of pressure ulcers to evaluate quality of provided care.* Dermatol Surg, 2009. **35**(11): p. 1797-803.
9. Stark, J.M., et al., *Detection of enhanced neutrophil adhesion to parainfluenza-infected airway epithelial cells using a modified myeloperoxidase assay in a microtiter format.* J Virol Methods, 1992. **40**(2): p. 225-42.
10. Tong, M., et al., *Stimulated neovascularization, inflammation resolution and collagen maturation in healing rat cutaneous wounds by a heparan sulfate glycosaminoglycan mimetic, OTR4120.* Wound Repair Regen, 2009. **17**(6): p. 840-52.
11. Woessner, J.F., Jr., *The determination of hydroxyproline in tissue and protein samples containing small proportions of this imino acid.* Arch Biochem Biophys, 1961. **93**: p. 440-7.
12. Garcia-Filipe, S., et al., *RGTA OTR4120, a heparan sulfate mimetic, is a possible long-term active agent to heal burned skin.* J Biomed Mater Res A, 2007. **80**(1): p. 75-84.
13. Tong, M., et al., *RGTA OTR 4120, a heparan sulfate proteoglycan mimetic, increases wound breaking strength and vasodilatory capability in healing rat full-thickness excisional wounds.* Wound Repair Regen, 2008. **16**(2): p. 294-9.

14. Tong, M., et al., *Heparan sulfate glycosaminoglycan mimetic improves pressure ulcer healing in a rat model of cutaneous ischemia-reperfusion injury.* Wound Repair Regen, 2011. **19**(4): p. 505-14.
15. Ledoux, D., et al., *Human plasmin enzymatic activity is inhibited by chemically modified dextrans.* J Biol Chem, 2000. **275**(38): p. 29383-90.
16. Meddahi, A., et al., *FGF protection and inhibition of human neutrophil elastase by carboxymethyl benzylamide sulfonate dextran derivatives.* Int J Biol Macromol, 1996. **18**(1-2): p. 141-5.
17. Melissa L. Petreaca, M.Y., Carl Ware, Manuela M. Martins-Green,, *Vascular endothelial growth factor promotes macrophage apoptosis through stimulation of tumor necrosis factor superfamily member 14 (TNFSF14/LIGHT).* Wound Repair and Regeneration, 2008. **16**(5): p. 602-614.
18. Widgerow, A.D., *Cellular/extracellular matrix cross-talk in scar evolution and control.* Wound Repair Regen, 2011. **19**(2): p. 117-33.
19. Alexakis, C., et al., *Reversal of abnormal collagen production in Crohn's disease intestinal biopsies treated with regenerating agents.* Gut, 2004. **53**(1): p. 85-90.
20. Schwentker, A., et al., *Nitric oxide and wound repair: role of cytokines?* Nitric Oxide, 2002. **7**(1): p. 1-10.
21. Boykin, J.V., Jr., *Wound nitric oxide bioactivity: a promising diagnostic indicator for diabetic foot ulcer management.* J Wound Ostomy Continence Nurs. **37**(1): p. 25-32; quiz 33-4.

Figure 1. Bodyweight measurement during diabetes induction (i.e. days 1-49 after STZ injection), ulceration and ulcer healing (i.e. days 49-134). Data are presented as means ± SEM. * $p < 0.05$ indicates significant difference in weight restoration after STZ injection between OTR4120-treated rats and control diabetic rats.

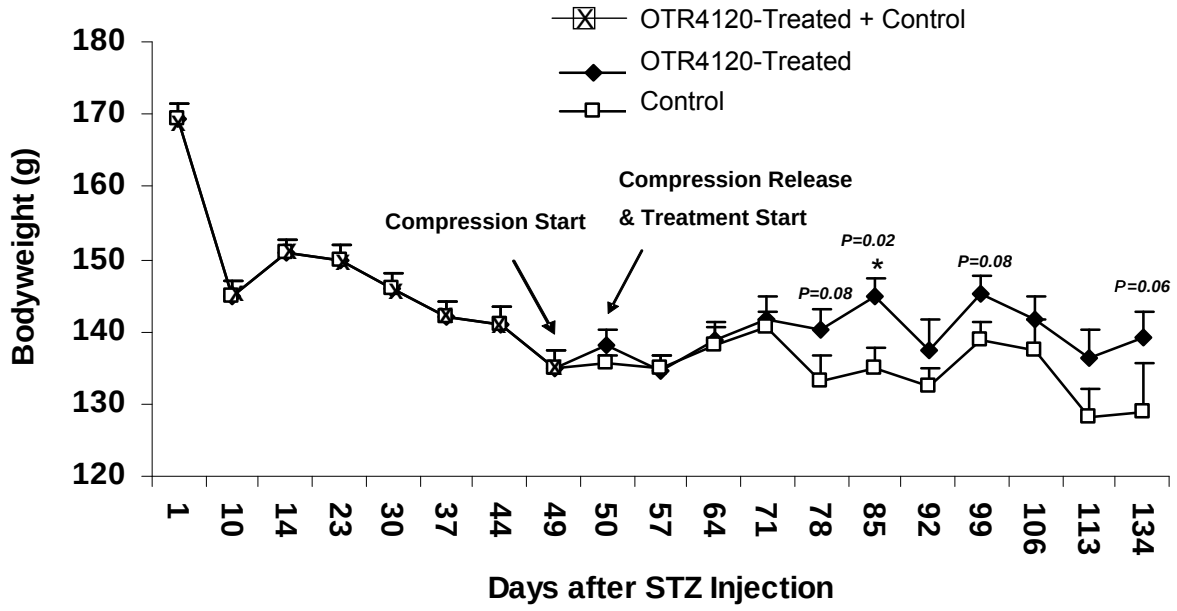

Figure 2. Macroscopic evaluation of the ulcer healing time in OTR4120-treated and control rats. Representative photographs (A) of ulcers in OTR4120-treated rats on day 14 (a), day 23 (b), and day 42 (c), and in control rats on day 14 (d), day 23 (e), and day 42 (f). Percentage of complete closed ulcers (B). * $p < 0.05$ indicates significant difference between the OTR4120-treated rats and control rats.

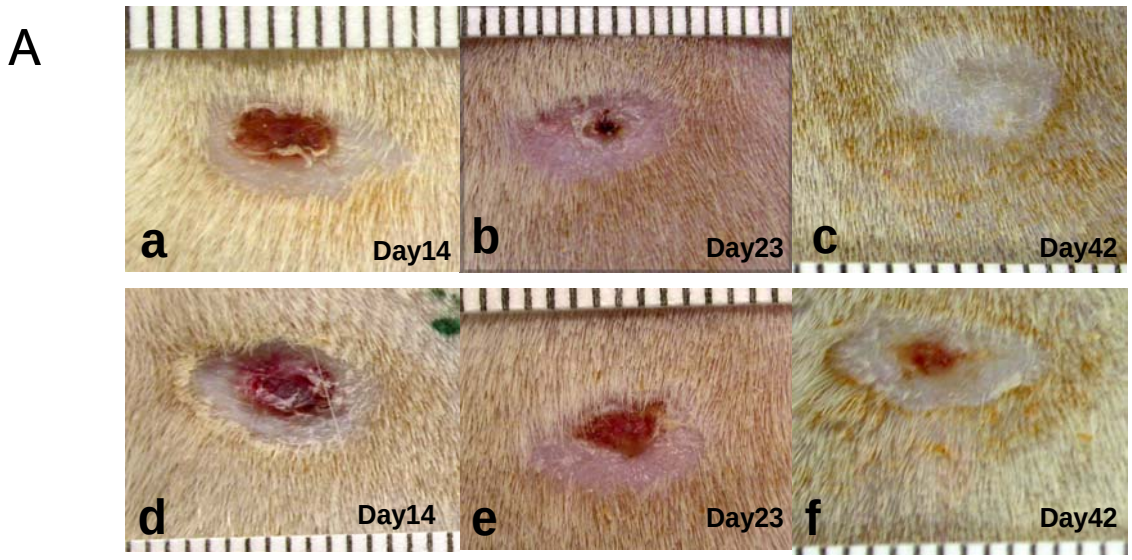

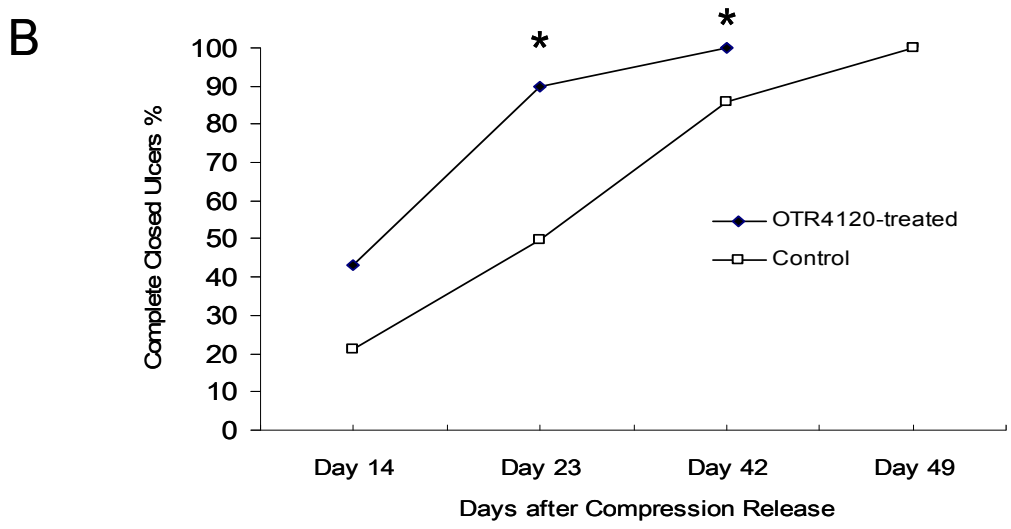

Figure 3. Effect of OTR4120 treatment on reducing neutrophil infiltration assessed by myeloperoxidase (MPO) activity assay (A) and hematoxylin and eosin (H&E) stained histology (B and C). Representative H&E staining section on day 7 after compression release of a control ulcer (B) shows intense infiltration of neutrophils (arrows) (magnification= X 1.25; scale bar = 4 mm) in the ulcer area, and an OTR4120-treated ulcer (C) shows less intense infiltration of neutrophils (arrows) (magnification= X 1.25; scale bar = 4 mm). Insert: top left images show normal skin tissue, located 2 mm from the ulcer margin of a control ulcer (B1) and an OTR4120-treated ulcer (C1) (magnification= X 10; scale bar = 500 μm). Insert: top right images show neutrophil infiltration at higher magnification of a control ulcer (B2) and an OTR4120-treated ulcer (C2) (magnification = X 40; scale bar = 100 μm). Data are presented as means ± SEM. *p < 0.05 and **p < 0.01 indicate significant differences between the OTR4120-treated groups and control groups.

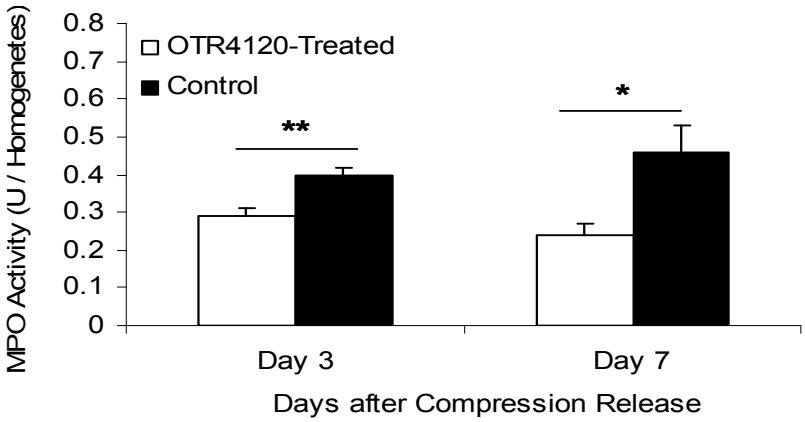

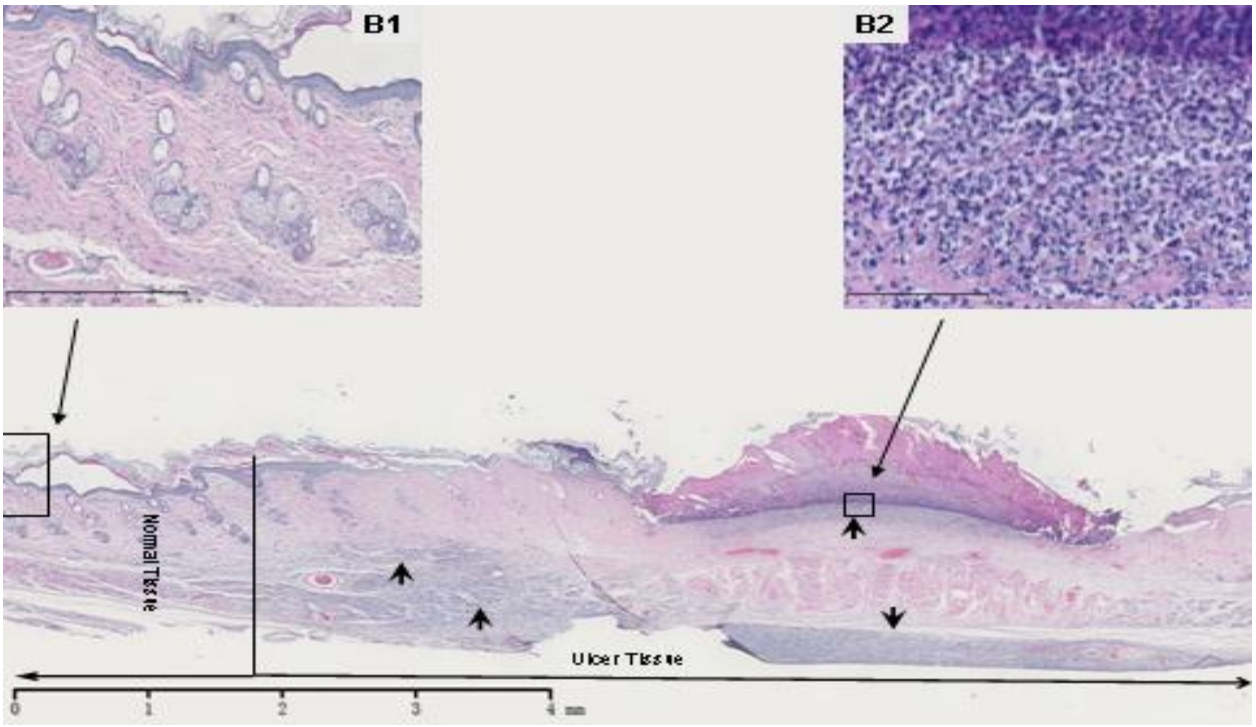
B1
B2
Normal Tissue
Ulcer Tissue
0
1
2
3
4 mm

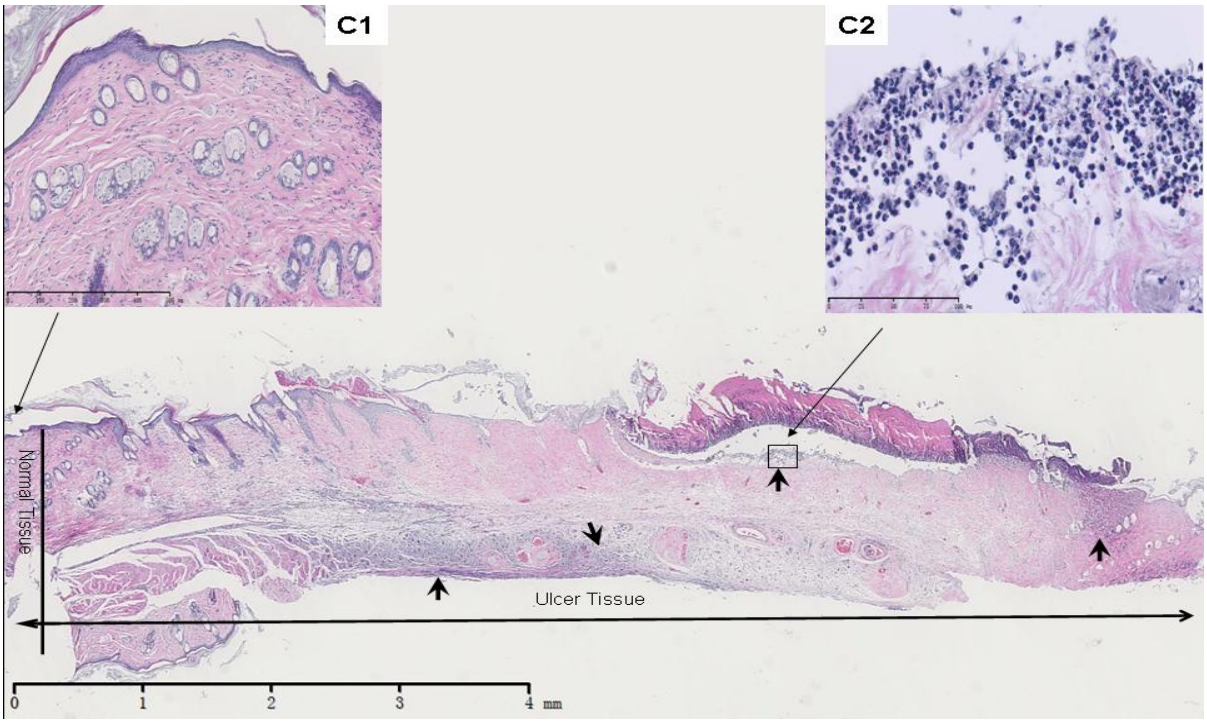
C1
C2
Normal Tissue
Ulcer Tissue
0
1
2
3
4 mm

Figure 4. Effect of OTR4120 treatment on inflammation reduction assessed by monocyte/macrophage marker CD68 immunohistochemistry. Representative CD68-staining sections of OTR4120-treated ulcers (A1-3) and control ulcers (B1-3) on days 7, 14, and 84 after compression release, respectively. Magnification = X 40. Insert magnification = X 200. Graphic visualization of scores of CD68-staining at indicated time points (C). Data are presented as means ± SEM. **p < 0.01 indicates significant difference between the OTR4120-treated groups and control groups.

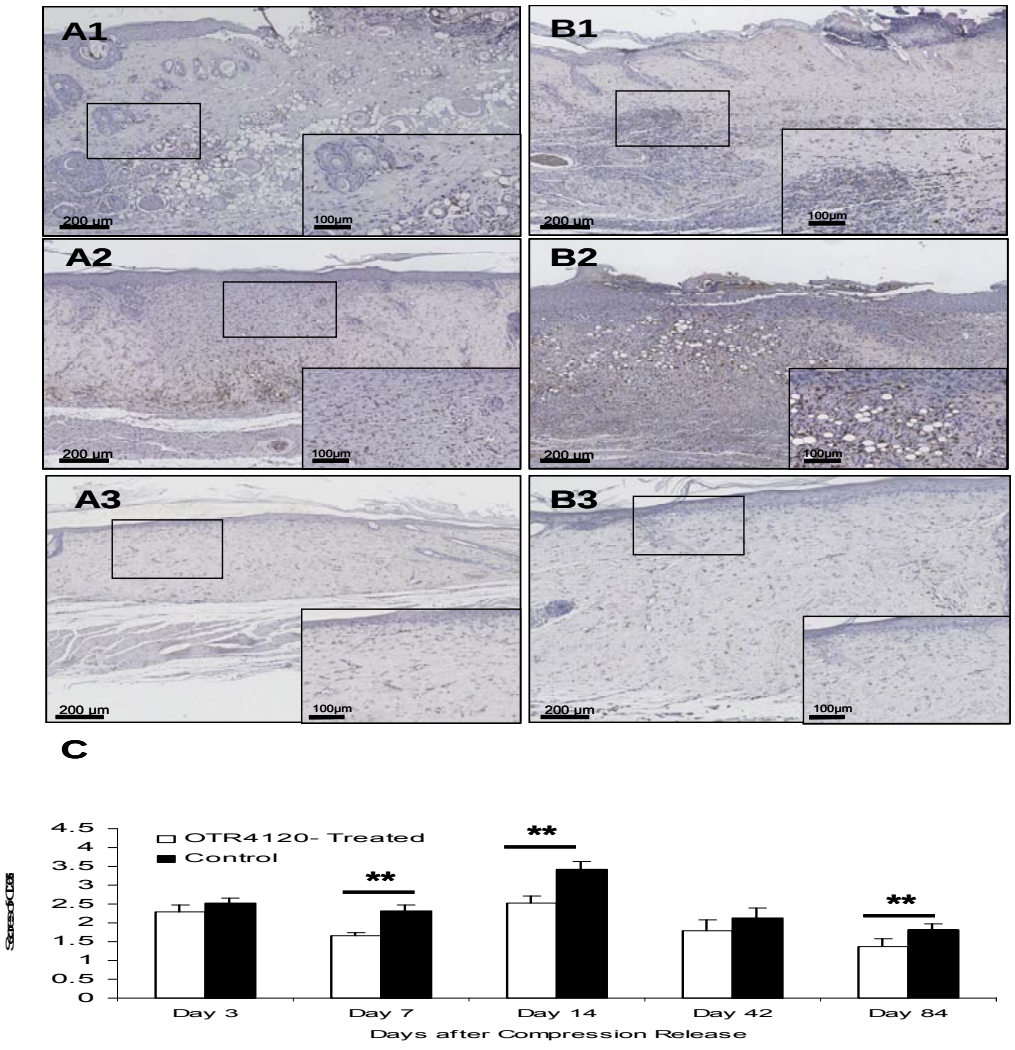

Figure 5. Effect of OTR4120 treatment on angiogenesis assessed by the endothelial cell marker CD34 immunohistochemistry. Representative CD34-staining sections of OTR4120-treated wounds (A1-2) and control wounds (B1-2) on days 14 and 42 after compression release, respectively. Magnification = X 40. Insert magnification = X 200. Graphic visualization of scores of CD34-staining at indicated time points (C). Data are presented as means ± SEM. **p < 0.01

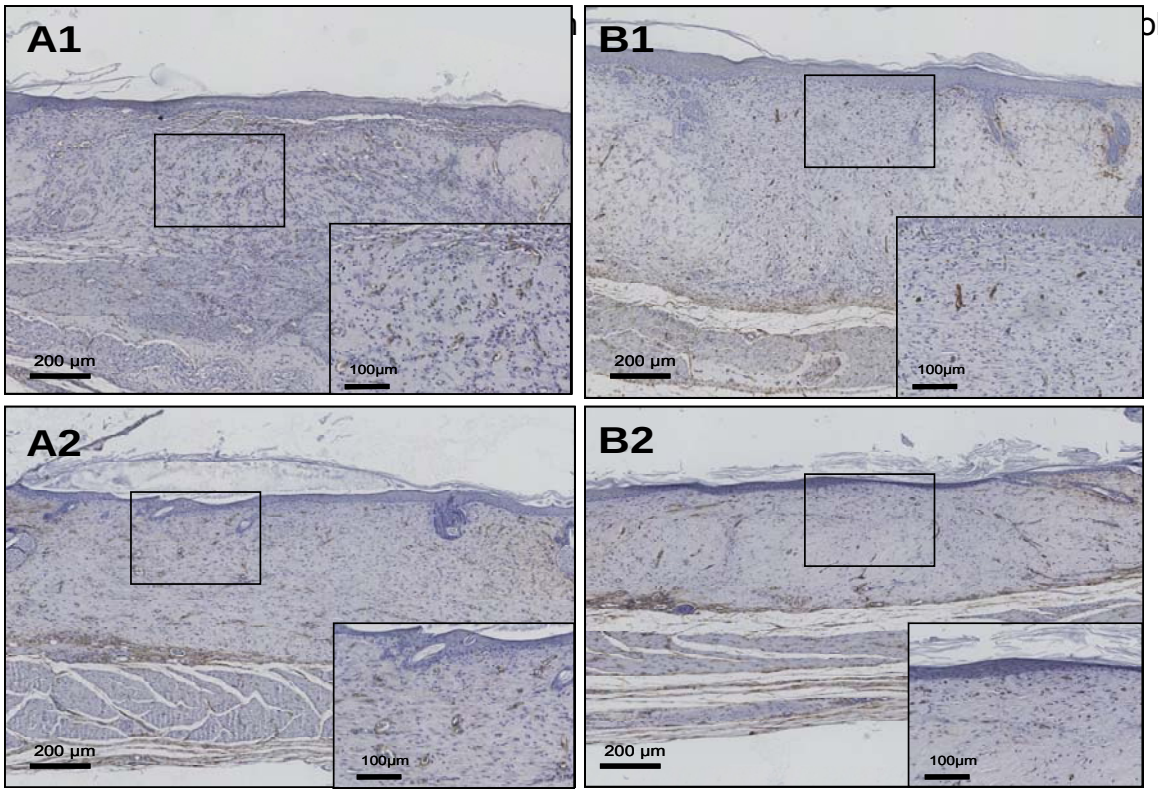

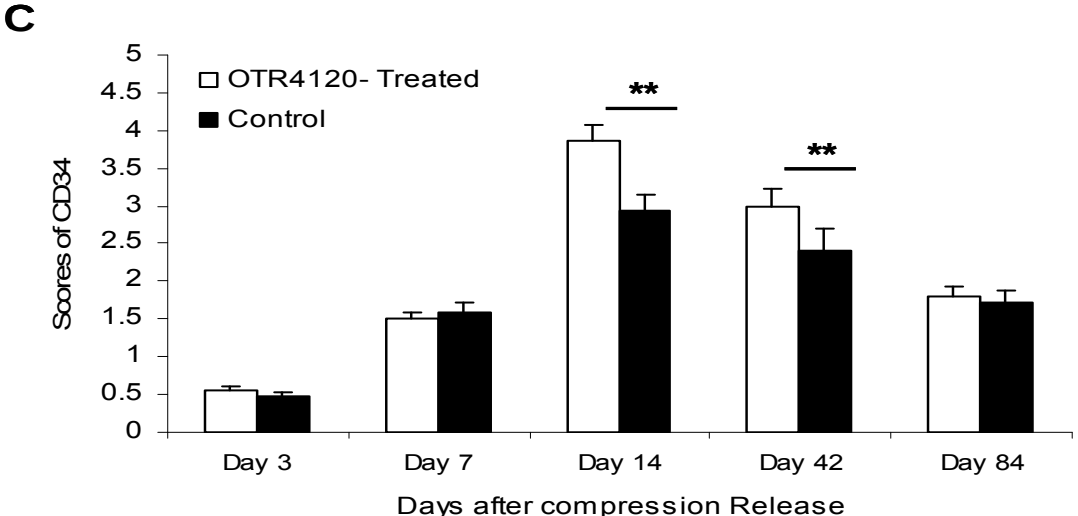

Figure 6. Effect of OTR4120 treatment on VEGF, TGF-β_1 , and iNOS protein contents as assessed by Western blot analysis. Representative bands of VEGF (A), TGF-β_1 (B), and iNOS (C) on days 3, 14, and 84 after compression release, respectively. Quantification of the VEGF bands (D), TGF-β_1 bands (E), and iNOS bands (F). Data are presented as means ± SEM. *$p < 0.05$, and **$p < 0.01$ indicate significant differences between the OTR4120-treated rats and control rats.

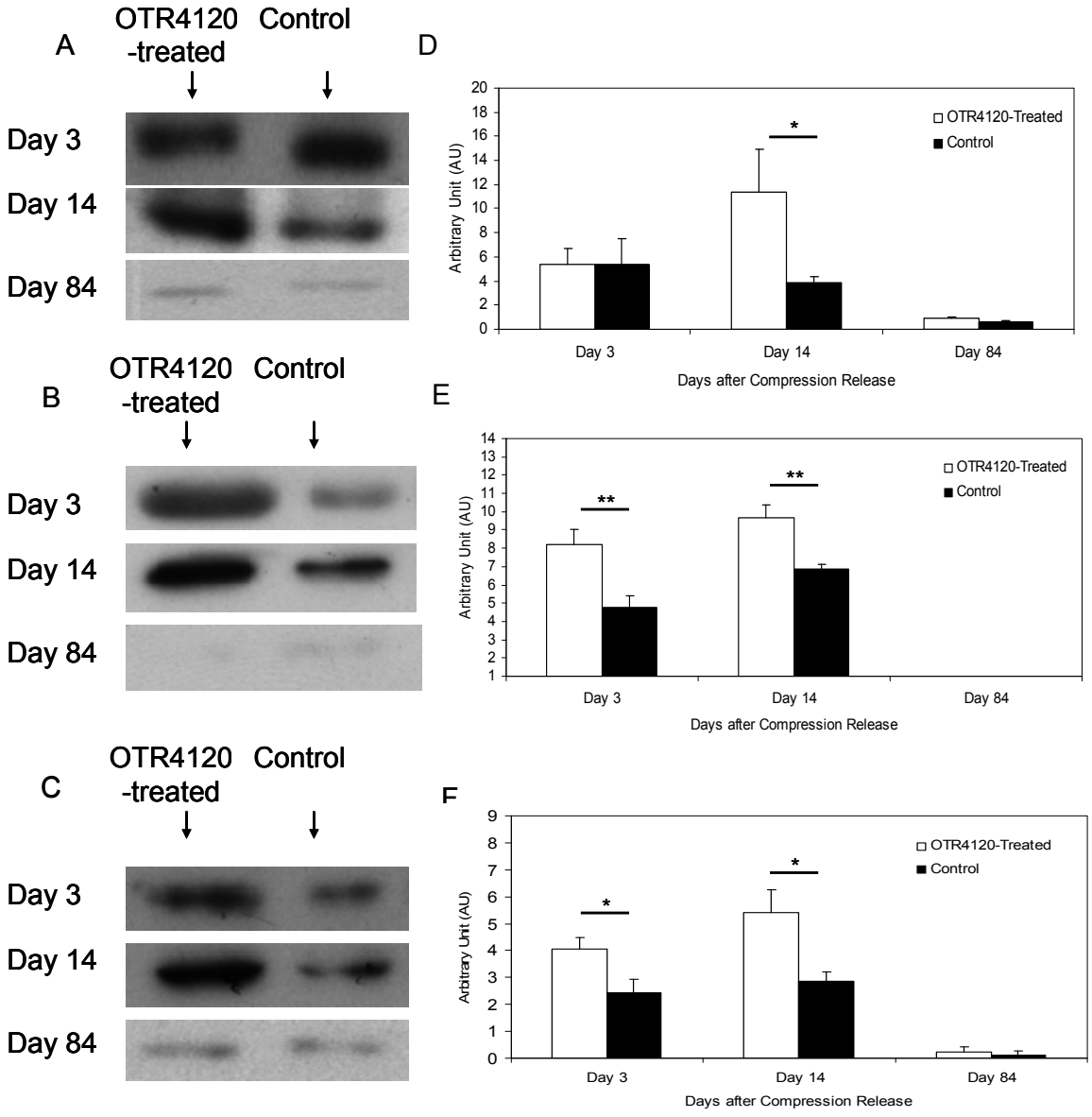

Figure 7. Ratio of the wound breaking strength of ulcer tissue compared to normal skin tissue on days 18, 42, and 84, respectively. Data are presented as means ± SEM. ***$p < 0.001$, **$p < 0.01$, and *$p < 0.05$ indicate significant differences between treated groups and control groups.

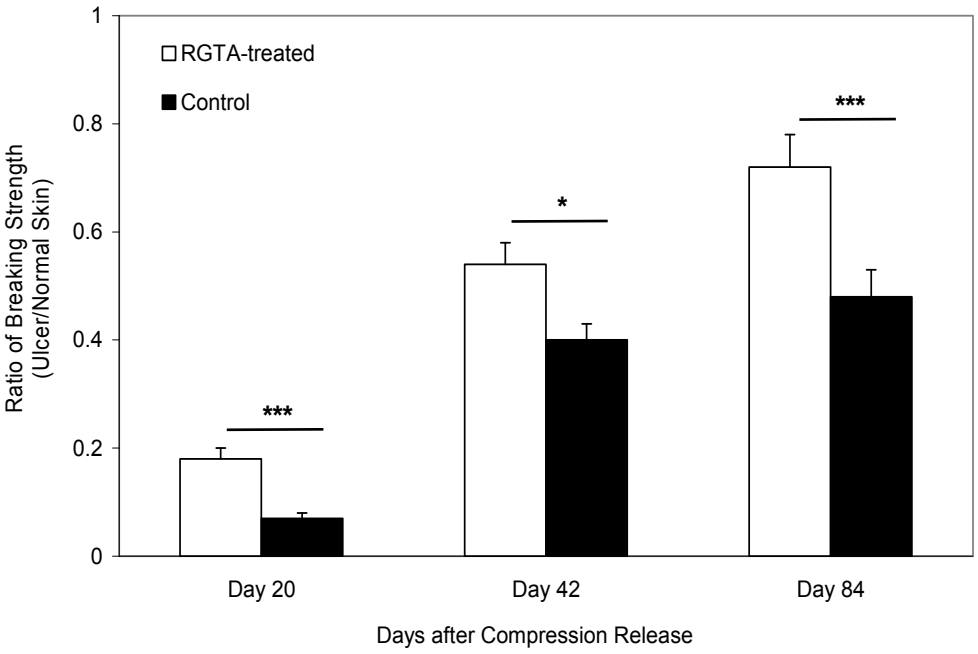

Figure 8. Biosynthesis of collagen type I and type III biosynthesis in ulcer tissue in control and OTR4120-treated rats. Ulcer tissue samples were ex vivo labeled with (^{3}H) hydroxyproline and digested by pepsin. Pepsin-soluble collagen types I and type III were determined by SDS-PAGE. The percentage of synthesized collagen type I to total synthesized collagen (A), the percentage of synthesized collagen type III to total synthesized collagen (B), and the ratio of collagen type

I/collagen type III (C). Data are presented as means ± SEM. *p < 0.05 indicates significant difference between treated groups and control groups.